

# The Composite Broad Band Spectrum of Cir X–1 at the Periastron: a Peculiar Z–source

R. Iaria<sup>1</sup>, L. Burderi<sup>2</sup>, T. Di Salvo<sup>1</sup>, A. La Barbera<sup>1</sup>, N. R. Robba<sup>1</sup>

## ABSTRACT

We report on the spectral analysis of the peculiar source Cir X–1 observed by the BeppoSAX satellite when the X–ray source was near the periastron. A flare lasting  $\sim 6 \times 10^3$  s is present at the beginning of the observation. The luminosity during the persistent emission is  $1 \times 10^{38}$  erg s $^{-1}$ , while during the flare is  $2 \times 10^{38}$  erg s $^{-1}$ . We produced broad band (0.1–100 keV) energy spectra during the flare and the persistent emission. At low energies the continuum is well fitted by a model consisting of Comptonization of soft photons, with a temperature of  $\sim 0.4$  keV, by electrons at a temperature of  $\sim 1$  keV. Out of the flare a power-law component, with photon index  $\sim 3$ , is dominant at energies higher than 10 keV. This component contributes to  $\sim 4\%$  of the total luminosity. During the flare its addition is not statistically significant. An absorption edge at  $\sim 8.4$  keV, with optical depth  $\sim 1$ , corresponding to the K-edge of Fe XXIII–XXV, and an iron emission line at 6.7 keV are also present. The iron line energy is in agreement with the ionization level of the absorption edge. The hydrogen column deduced from the absorption edge is  $\sim 10^{24}$  cm $^{-2}$ , two order of magnitude larger than the absorption measured in this source. We calculated the radius of the region originating the comptonized seed photons,  $R_W \sim 150$  km. We propose a scenario where  $R_W$  is the inner disk radius, a highly ionized torus surrounds the accretion disk and a magnetosphere is large up to  $R_W$ . The absorption edge and the emission line could originate in the photoionized torus, while the comptonized component originates in an inner region of the disk.

*Subject headings:* stars: individual: Cir X–1 — stars: neutron stars — X-ray: stars — X-ray: spectrum — X-ray: general

## 1. Introduction

Circinus X–1 (Cir X–1) is one of the most enigmatic X–ray binary sources and shows a complex temporal and spectral behaviour. The earliest unambiguous X–ray detection was made by Margon

---

<sup>1</sup>Dipartimento di Scienze Fisiche ed Astronomiche, Università di Palermo, via Archirafi n.36, 90123 Palermo, Italy

<sup>2</sup>Osservatorio Astronomico di Roma, Via Frascati 33, 00040 Monteporzio Catone (Roma), Italy

et al. (1971). The position of the probable radio counterpart is located near the supernova remnant G321.9–0.3 (Clark, Parkinson & Caswell, 1975), suggesting that Cir X–1 could be a runaway binary. The source displays a periodicity at radio (Whelan et al., 1977), IR (Glass, 1978), optical (Moneti, 1992) and X–ray wavelengths (Kaluzienski et al. 1976) with a period of  $\sim 16.6$  days. The high degree of stability of this period suggests that it is the orbital period. Periodic radio flares near the zero phase (for recent ephemeris see Stewart et al., 1991) of the orbital period are also accompanied by drastic changes in the X–ray light curve (X–ray flares and dips). These variations can be explained in terms of a highly eccentric binary orbit, where the periastron, and consequently the increased mass transfer, occur near zero phase (Murdin et al. 1980). Shirey (1998) observed that the dipping activity of Cir X–1 occurs within 0.03 and 0.09 in the phase interval when the source enters its flaring state, after an increase of intensity in the X–ray light curve (Brandt et al., 1996; Shirey et al., 1996). These dips might be explained by obscuration due to inhomogeneities in the mass transfer stream or intermittent bumps on the outer edge of the accretion disk (Shirey, 1998). There is evidence of presence of radio jets from the source (Stewart et al., 1993).

Cir X–1 shows a long-term variability in its luminosity. EXOSAT observations show a gradual increase in the brightness of the source near zero phase from 1984 to 1986, models involving the precession of the accretion disk, the thickening of the outer disk, or an apsidal motion have been proposed (Oosterbroek et al., 1995).

The optical counterpart of Cir X–1 is a faint red star (Moneti, 1992). The large ratio  $L_x/L_{opt}$  suggests that Cir X–1 is a low–mass X–ray binary (LMXB). For a long time it was suspected that the compact object in Cir X–1 was a black hole, for the rapid variability similar to that of Cyg X–1 (Toor, 1977). However the presence of a neutron star was demonstrated by the detection of type I X–ray burst (Tennant et al., 1986 a,b). The spectral and fast timing properties of accreting low magnetic field neutron stars permit to distinguish them into two class, Z and Atoll sources, from the pattern each source describes in a X–ray color–color diagram (Hasinger & van der Klis, 1989). The Z–sources are very bright and could have a moderate magnetic field, while the Atoll–sources have a lower luminosity and probably a weaker magnetic field. It was not clear what kind of LMXB Cir X–1 is. Oosterbroek et al. (1995) proposed that Cir X–1 may be an Atoll–source with a magnetic field strength of less than  $10^9$  Gauss. Using RXTE data Shirey (1998) identified much of the behaviour of Cir X–1 as that of a Z–source: hardness–intensity diagrams showed that the track differs somewhat from the canonical Z track, but the temporal behaviour of the source along the branches strongly suggests that Cir X–1 is a Z–sources. The presence of horizontal–branch oscillations, in the range 1–20 Hz, in the framework of the beat–frequency model (Alpar & Shaman, 1985; Lamb et al., 1985), could indicate a significant magnetic field. Quasi periodic oscillations (QPO) at 100–200 Hz have been reported (Tennant, 1987; Shirey et al., 1996; Shirey, 1998), but no kHz QPOs were detected.

The distance to Cir X–1 was estimated to be between 8–10 kpc (Goss & Mebold, 1977). Recently, Case & Bhattacharya (1998) have revised the distance to the supernova remnant G321.9–0.3, and hence to the associated Cir X–1, to 5.5 kpc. In the following we adopt 5.5 kpc as the

distance to the source, unless otherwise stated.

The spectrum of Cir X–1 has been poorly understood up to now. ASCA data taken near the zero phase, at a low count rate, have been fitted with an absorbed two–blackbody model (Brandt *et al.*, 1996). An iron K edge at 7 keV was present, that corresponds to a large absorption column of  $\sim 10^{24}$  cm $^{-2}$  and can be explained by a partial covering model. A weak emission line at 6.4 keV has also been detected. The edge and the gaussian emission line were no longer detected at higher count rate, above 300 c s $^{-1}$  (Brandt *et al.*, 1996). In a recent RXTE observation (Shirey *et al.*, 1999a) the spectrum of Cir X–1 was fitted using the Eastern Model (Mitsuda *et al.*, 1984), i.e. a multicolor disk blackbody, with a temperature between 1.2–1.4 keV, and a blackbody with a temperature in the interval 1.9–2.4 keV. They found a peculiar feature, very prominent in the flaring branch, around 10 keV not easily understandable. This feature could be fitted with an absorption edge, but even a narrow line improved the fit.

Here we report the results of a broad band (0.1–100 keV) spectral analysis performed on Cir X–1 data from the BeppoSAX satellite. The broad energy coverage of BeppoSAX narrow field instruments allows us to well constrain the spectrum of this source, and to detect the presence of a high energy component.

## 2. Observations and Light Curve

The Narrow Field Instruments (NFI) on board BeppoSAX satellite (Boella *et al.* 1997) observed Cir X–1 from 1998 August 1 15:59:54.5 UT, for a total time of 90 ks. The NFIs are four co-aligned instruments which cover more than three decades of energy, from 0.1 keV up to 200 keV, with good spectral resolution in the whole range. LECS (operating in the range 0.1–10 keV) and MECS (1–11 keV) have imaging capabilities with a field of view of 20' and 30' radius, respectively. We selected the data for scientific analysis in circular regions, centered on the source, of 8' and 4' radii for LECS and MECS respectively. The background subtraction was obtained using blank sky observations in which we extracted the background spectra in regions of the field of view similar to those used for the source. HPGSPC (7–60 keV) and PDS (13–200 keV) have not imaging capabilities, because their field of views, of  $\sim 1^\circ$  FWHM, are delimited by collimators. The background subtraction for these instruments is obtained using the off-source data accumulated during the rocking of the collimators. The energy ranges used in the spectral analysis are: 0.12–4 keV for LECS, 1.8–10.5 keV for MECS, 7–25 keV for HPGSPC and 15–100 keV for PDS. LECS was only active in the time interval between  $3.4 \times 10^4$  s and  $\sim 5.9 \times 10^4$  s from the beginning of the observation. Different normalizations of the NFIs are considered by including in the model normalizing factors, fixed to 1 for MECS, and kept free for the other instruments. A systematic error of 2% was added to the spectra. Assuming the orbital ephemeris as reported by Stewart *et al.* (1991), we find that our observation covers the phase interval from 0.11 to 0.16.

In Figure 1 we plotted the Cir X–1 light curve in the energy band 1.8–10 keV (MECS data,

upper panel), and the ratio of the count rate in the energy band 3–7 keV to that in the band 1–3 keV (lower panel). No dips are present in the light curve. A flare that lasts  $\sim 6 \times 10^3$  s is present. The average count rate, out of the flare, is  $\sim 300$  counts/s in the MECS, corresponding to an average hardness ratio of  $\sim 0.6$ . The count rate increases during the flare, reaching  $\sim 700$  counts/s at the peak, where the hardness ratio is  $\sim 0.9$ . We also observe that the hardness ratio increases from the end of the flare to the end of the observation (see Fig. 1). We plotted in Figure 2 the color-color diagram (hereafter CCD) of the source using a bin time of 137 s. The variations are mainly due to the presence of the flare. The shape of this CCD is reminiscent of the flaring branch observed in the Z-Sources. We divided our observation in 8 intervals as reported in Table 1 and in Fig. 1. The first five intervals are taken during the flare in order to study the rapid spectral variation. The last three intervals are taken out of the flare and correspond to different hard colors and positions in the CCD.

In Table 1 we show the flux of the source in the 2.5–25 keV energy range for all the intervals in order to compare these values with previous observations. In the same table we report the average observed flux of the source in the 0.1–100 keV energy range, and the corresponding luminosity of the source. The LECS data are not always available; in Table 1 we report for which intervals LECS was active.

### 3. Spectral Analysis

As described above we extracted five spectra during the flare and three spectra during the persistent emission corresponding to different hard colors. The LECS was active only in two of the eight intervals (see Tab. 1). The average photoelectric absorption by cold matter, obtained fitting the spectra containing the low energy data, is  $\sim 1.74 \times 10^{22}$  cm $^{-2}$ . This parameter was fixed in the other intervals. A simple model, such as a blackbody or a disk multicolor blackbody, plus photoelectric absorption by cold matter, is not sufficient to fit the data. The spectra during the flare at higher count rate (intervals from 2 to 4) and the soft part (up to 10 keV) of all the other spectra are well fitted by a comptonized model (*Comptt*, Titarchuk 1994), the Comptonization of soft seed photons in a Wien distribution by hot electrons. We obtained seed-photon and electronic temperatures of  $\sim 0.4$  keV and  $\sim 0.9$  keV, respectively, and both seem to increase during the flare (see Fig. 4). The Compton optical depth is around 17 for all the spectra. A blackbody plus a disk multicolor blackbody give equivalent fits. In this case we obtain a disk temperature of  $\sim 0.4$  keV, similar to the seed photon temperature and a blackbody temperature of  $\sim 0.9$  keV, corresponding to the electronic temperature of the Comptonization model.

The spectra at lower count rate (intervals 1, 5, 6, 7, 8) show a marked hard excess above 10 keV with respect to the previous models. The addition of a power law to the model improves the fit with very high statistical significance, although a thermal-bremsstrahlung component instead of the power law can not be excluded. The power-law component contributes to  $\sim 4\%$  of the total luminosity and its photon index is between 3.17 and 3.37. We also added the hard power-law

component to the other spectra at high count rate (intervals 2, 3, 4), fixing the photon index to the average value 3.3. In these cases, the power-law component does not improve the fit, and we obtain an upper limit on the normalization. In Table 2 and 3 we report the result of the fits for all the intervals and the probability of chance improvement for the addition of a power law component.

A feature between 8 and 10 keV is clearly visible in all the spectra and was also present in previous observations (e.g. Shirey et *al.*, 1999a). We add an edge at  $\sim 8.4$  keV to fit this feature improving the fits with high statistical significance. In spectra 6, 7, 8 the addition of an iron line improves furtherly the fit (the addition is significant at a confidence level between 99.8% and 99.996%). The iron line energy is  $\sim 6.7$  keV, with an upper limit for sigma of 0.24 and 0.47 keV (spectra 6 and 7 respectively), and a sigma of 0.5 keV for spectrum 8. We find that the equivalent widths are between 46 and 100 eV (see Table 3). In Figure 3 we report the spectra and the residuals in units of  $\sigma$  with respect to the best fit model for intervals 4 (at the peak of the flare) and 6 (out of the flare). In Figure 4 we report the unfolded spectrum for the same intervals shown in Figure 3.

#### 4. Discussion

We analyzed data of Cir X-1 from a BeppoSAX 90 ks observation in the energy range 0.1–100 keV. The light curve shows a flare lasting  $\sim 6 \times 10^3$  s at the beginning of the observation and does not show dipping activity. The CCD of the source that we obtained is similar to the FB of a typical Z-source, in line with RXTE results (Shirey et *al.*, 1998; 1999a).

The equivalent absorption column  $N_H$  is  $\sim 1.74 \times 10^{22}$  cm $^{-2}$ , and is in agreement with previous observations (Brandt et *al.*, 1996). For a distance to the source of 5.5 kpc (Case & Bhattacharya, 1998) the visual extinction in the direction of Cir X-1 is  $A_v = 5.8 \pm 2.0$  mag (Hakkila et al. 1997). Using the observed correlation between visual extinction and absorption column (Predehl & Schmitt 1995) we find  $N_H = (1.38 \pm 0.02) \times 10^{22}$  cm $^{-2}$ . It is slightly smaller than the value obtained from the fit, probably because of the presence of obscuring matter close to the X-ray source.

A comptonized spectrum with an iron absorption edge are needed to fit the broad band energy spectra. For the spectra with lower count rate (intervals 1, 5, 6, 7, 8) the addition of an extra hard component is needed to fit the high energy range. The temperatures of the seed photons and the hot electrons of the comptonized component increase during the flare. In Figure 5 we plotted the two temperature versus the time (centers of the corresponding temporal intervals). The optical depth of the comptonizing region is  $\sim 17$  and does not seem to vary. The unabsorbed luminosity of comptonized component is  $\sim 2 \times 10^{38}$  erg s $^{-1}$  during the persistent emission, and reaches  $\sim 3.5 \times 10^{38}$  erg s $^{-1}$  at the peak of the flare. In Figure 6 we report the electronic temperature versus the seed-photon temperature. A linear correlation between the two temperatures is evident, with a slope of  $3.2 \pm 1.2$ . This correlation could indicate a sort of equilibrium between the two

temperatures, because an increase of the seed-photon temperature corresponds to an increase of the electron temperature. The comptonizing region is probably located in the inner part of the system, covering part of the accretion disk, where the seed photons could originate.

An Eastern model (blackbody plus multicolor disk blackbody) instead of a comptonized model also fits well the data. The inner radius of the disk that we obtain in this case is  $\sim 160$  km, assuming an inclination angle of  $60^\circ$ , similar to the radius of the seed photons obtained from the previous model (see below). On the other hand the radius of  $\sim 35$  km obtained from the blackbody is quite large to be identified with the neutron star radius. It is possible that the blackbody mimics the Wien law of the Comptt model. Because the Comptt model seems more reasonable we adopt this interpretation.

#### 4.1. Possible presence of a magnetic field of $\sim 4 \times 10^{10}$ Gauss

For each interval we calculated the radius of the seed-photon Wien spectrum,  $R_W$ , using the parameters reported in Tables 2 and 3. Following in 't Zand et al. (1999) this radius can be expressed as  $R_W = 3 \times 10^4 D \sqrt{\frac{f_{bol}}{1+y}} / (kT_0)^2$  km, where  $D$  is the distance to the source in kpc,  $f_{bol}$  is the unabsorbed flux of the Comptt model in  $\text{erg cm}^{-2} \text{s}^{-1}$ ,  $kT_0$  is the seed photon temperature in keV, and  $y = 4kT_e\tau^2/m_e c^2$  is the relative energy gain due to the Comptonization. We obtain that the seed-photon radius is  $\sim 150$  km. An hypothesis is that this is the inner radius of the accretion disk. It is quite large but we observe that a large inner disk radius is in agreement with the absence of kHz QPOs in the power spectrum density of Cir X-1 (Shirey et al., 1996). In fact kHz QPOs are usually explained as the Keplerian frequency at the inner edge of the disk, near the neutron star surface (Strohmayer et al. 1996; Miller, Lamb, & Psaltis 1998; Stella & Vietri 1999; Titarchuk, Lapidus, & Muslimov 1998). The lack of kHz frequencies in the power spectra of Cir X-1 could mean that the inner region of the disk is not present.

A possible explanation of the large value of the inner radius is that the compact object presents a magnetic field sufficiently strong to obtain a magnetosphere around the neutron star, although in this case we need to suppose a particular geometrical configuration in order to avoid the unobserved coherent pulsations. The relation between the magnetospheric radius  $R_m$  and the magnetic field strength is  $R_m = 4.3 \times 10^3 \phi \mu_{30}^{4/7} R_6^{-2/7} L_{37}^{-2/7} \epsilon^{2/7} m^{1/7}$  km (see e.g. Burderi et al., 1998), where  $\phi \sim 0.5$  is a correction factor for the Alfvén radius when an accretion disk is present (Ghosh & Lamb, 1991),  $\mu_{30}$  is the magnetic moment in units of  $10^{30}$  G cm<sup>3</sup>,  $R_6$  is the neutron star radius,  $R_{NS}$ , in units of  $10^6$  cm,  $\epsilon = GM\dot{M}/R_{NS}$  is the ratio between the observed luminosity and the total gravitational potential energy released per second by the accreting matter,  $m$  is the neutron star mass in unit of solar mass. Adopting  $R_6 = 1$  and  $m = 1.4$  (typical for a neutron star),  $\epsilon \sim 1$ ,  $L_{37}$  is the intrinsic luminosity of the comptonized component in units of  $10^{37}$  erg s<sup>-1</sup>, and  $R_m = R_W$  we can find a magnetic field strength for each interval. The obtained values are consistent with an average magnetic field of  $\sim 4 \times 10^{10}$  Gauss. This value is slightly higher than the typical magnetic

field strength inferred for the Z–sources.

Another possibility to explain the large inner radius of the accretion disk is that the inner region of the disk is hidden for the presence of optically thick material (e.g. the comptonized region with Compton optical depth  $\sim 17$ ) in the central part of the system.

#### 4.2. Detection of a hard tail in the energy spectra

A hard component is required to fit the spectra at low luminosity (1, 5, 6, 7, 8). During the flare the hard component is not detected with statistical significance (see Tab. 3, where the upper limit for the normalization is reported). A similar hard component has also been observed in GINGA data of GX 5–1 (Asai *et al.*, 1994), in BeppoSAX data of GX 17+2 (Di Salvo *et al.*, 2000) and in BeppoSAX data of GX 349+2 (Di Salvo *et al.*, 2000b). Asai *et al.* (1994) observed GX 5–1 in the normal branch (NB) and in the flaring branch (FB) of the relative Z-track; the intensity of the power-law component decreases from the NB to the FB. Di Salvo *et al.* (2000) observed GX 17+2 in the horizontal branch (HB) and in the NB, and the intensity of the power-law component was found to decrease toward the NB/FB vertex. In Cir X–1 the intensity of the power-law component decreases from the NB/FB vertex toward the FB.

The hard excess could have a non thermal origin, due to scattering of soft photons by electrons with a non thermal distribution of velocities. These electrons could be part of a jet. In fact Stewart *et al.* (1993) detected the presence of a jet with a maximum at the phase 0.17 where the flux increased up to 12 mJy and an upper limit on the 12-h integrated flux density of  $\sim 3 \pm 1$  mJy. The angle between the jet and the line of sight is  $> 70^\circ$  (Stewart *et al.*, 1993; Fender *et al.*, 1998). Our observation is in the phase interval 0.11–0.16, near the observed maximum of the radio flux. So, a jet could be the origin of the power law observed in Cir X–1, and similarly in GX 5–1 and GX 17+2. These sources, as well as all the Z–sources, have been associated with variable radio sources (Fender & Hendry 2000, and reference therein). Note that these hard component might be a general feature of the Z–sources and this is another feature that Cir X–1 shares with the Z–source family.

#### 4.3. Could an ionized torus be present around the disk?

An absorption edge at  $\sim 8.4$  keV is present in all the spectra, and a gaussian emission line at  $\sim 6.7$  keV is detected in the spectra 6, 7 and 8 (see Tab. 2 and 3). The energy of the emission line is compatible with the iron ionization levels Fe XXIII–XXV indicated by the absorption edge energy (see Turner *et al.*, 1992 for a correspondence between iron edge energy and ionization level). The best fit value for the optical depth  $\tau_{edge}$ , considering the photoionization cross section for the K–shell Fe XXIII (Krolik & Kallman, 1987), corresponds to a hydrogen column density of  $\sim 1.5 \times 10^{24}$  cm $^{-2}$ , assuming a cosmic abundance of iron. This is much higher than the measured

photoelectric absorption (see Tab. 2 and 3). This could imply the existence of a highly ionized region around the compact object, producing the absorption edge and not contributing to the photoelectric absorption. In ASCA observations Brandt *et al.* (1996) observed an iron edge at  $\sim 7.1$  keV. To explain the presence of this edge they discussed that a poorly ionized torus could be present around the neutron star, finding the relative covering fraction of  $\sim 94\%$  when the absorbed flux was  $\sim 1.5 \times 10^{-9}$  erg cm $^{-2}$  s $^{-1}$  (low state). When the absorbed flux was  $\sim 2.4 \times 10^{-8}$  erg cm $^{-2}$  s $^{-1}$  (high state), the partial covering and the edge at 7 keV were no longer detected. Their measures of the galactic  $N_H$ ,  $\sim 1.77 \times 10^{22}$  cm $^{-2}$ , and the partial covering  $N_H$ ,  $\sim 1.5 \times 10^{24}$  cm $^{-2}$ , are in agreement with our results. Shirey *et al.* (1999a) observed a feature at 10 keV, present in the flaring branch during the high state of the source. In our observation the absorbed flux is  $\sim 2 \times 10^{-8}$  erg cm $^{-2}$  s $^{-1}$  (high state), and the energy of the edge is high, similar to the value obtained by Shirey *et al.* (1999a).

The torus of matter around Cir X-1 could be a deformation of the outer region of the accretion disk due to the tidal interaction between the two stars of the binary system and to the high mass transfer from the donor star. When Cir X-1 is in a low state the torus is poorly ionized, and it partially absorbs the spectrum, and an edge from neutral iron and a fluorescence line at 6.4 keV are present. When Cir X-1 is in a high state the torus could be photoionized, it is not necessary to use a partial covering to fit the data, an emission line at 6.7 keV is present and the absorption edge is shifted to higher energies. The angle between the jet and the line of sight is probably  $> 70^\circ$  (Fender *et al.*, 1998). Assuming that the direction of the jet is perpendicular to the plane of the disk then the angle between the plane of the disk and the line of sight is  $< 30^\circ$ . This could support the hypothesis that the line of sight intercepts the torus.

In the hypothesis that the thickness of the torus is much less than  $d$ , its distance from the source, we can estimate a constraint on the distance of the torus from the neutron star  $d < L/N\xi$  (Reynolds & Fabian, 1995), where  $L$  is the unabsorbed luminosity,  $N$  is the column density of photoionized matter, and  $\xi$  measures the ionization level. In order to have Fe XXIII the ionization parameter is  $\xi \sim 100$  erg cm s $^{-1}$  (Turner *et al.*, 1992). For  $L \sim 2 \times 10^{38}$  erg s $^{-1}$  and  $N$ , the column density of photoionized matter,  $\sim 1.5 \times 10^{24}$  cm $^{-2}$  we obtain  $d < 10^{12}$  cm. Considering that the minimum distance between the two stars of the binary has an upper limit of  $\sim 6 \times 10^{11}$  cm (Murdin *et al.*, 1980) we have only a weak constraint that the torus is within the system.

## 5. Conclusions

We analyzed data from a BeppoSAX observation of Cir X-1 performed in 1998 August 1. During the observation a flare lasting 6000 s was present. The energy spectrum is described by a Comptonized model, with a seed-photon temperature of  $\sim 0.4$  keV and electron temperature of  $\sim 0.9$ . A hard power-law component is present in the spectra out of the flare. The radius of the seed-photon Wien distribution is  $\sim 150$  km. The comptonized spectrum is produced in a relatively cool ( $\sim 1$  keV) region of moderate optical depth ( $\tau \sim 17$  for a spherical geometry). The power-law

component, probably produced by scattering on high energy electrons in a jet, has a photon index of  $\sim 3$ . We observe an absorption edge at  $\sim 8.4$  keV, probably originating from Fe XXIII. Its optical depth requires  $N_H \sim 1.5 \times 10^{24}$  cm $^{-2}$ , probably due to a highly ionized torus around the accretion disk. In the spectra out of flare we observe an iron emission line at 6.7 keV, with equivalent widths  $\sim 40 - 100$  eV whose energy indicates a high ionization level in agreement with that of the iron edge.

This work was supported by the Italian Space Agency (ASI), by the Ministero della Ricerca Scientifica e Tecnologica (MURST).

## REFERENCES

Alpar, M., Shaham, J., 1985, *Nature*, 316, 239

Asai, K., Dotani, T., Mitsuda, K., Nagase, F., Kamado, Y., Kuulkers, E., Breedon, L. M., 1994, *PASJ*, 46, 479

Boella G., Butler R. C., Perola G. C., Piro L., Scarsi L., Blecker J., 1997, *A&AS*, 122, 299

Brandt, W. N., Fabian, A. C., Dotani, T., Nagase, F., Inoue, H., Kotani, T., Segawa, Y., 1996, *MNRAS*, 283, 1071

Burderi, L., Di Salvo, T., Robba, N. R., Del Sordo, S., Santangelo, A., Segreto, A., 1998, *ApJ*, 498, 831

Case, G. L., Bhattacharya, D., 1998, *ApJ*, 504, 761

Clark, D. H., Parkinson, J. H., Caswell, J. L., 1975, *Nature*, 254, 674

Di Salvo T. et al., 2000, *ApJL* accepted

Di Salvo T. et al., 2000b, *ApJL* in preparation

Fender, R. P., et al., 1998, *ApJ*, 506, L121

Fender, R. P., Hendry, M. A., 2000, *MNRAS*, 317, 1

Glass, I. S., 1978, *MNRAS*, 183, 335

Ghosh, P., Lamb, F. K., 1991, in *Neutron Stars: Theory and Observation*, ed. J. Ventura & D. Pines (NATO ASI Ser. C, 344; Dordrecht: Kluwer), 363

Goss, W. M., Mebold, U., 1977, *MNRAS*, 181, 255

Hakkila J., Myers J. M., Stidham B. J., Hartmann D. H., 1997, *AJ*, 114, 2043

Hasinger, G., van der Klis, M., 1989, *A&A*, 225, 79

in 't Zand, J. J. M. et al., 1999, *A&A*, 345, 100

Kaluzienski, L. J., Holt, S. S., Boldt, E. A., Selermitsos, P. J., 1976, *ApJL*, 191, L71

Krolik, J. H., Kallman T. R., 1987, *ApJL*, 320, L5

Lamb, F. et al., 1985, *Nature*, 317, 681

Margon, K. O., Lampton, M., Bowyer, S., Cruddace R., 1971, *ApJL*, 169, L23

Miller, M. C., Lamb, F. K., Psaltis, D. 1998, *ApJ*, 508, 791

Mitsuda, K., et al., 1984, PASJ, 36, 741

Moneti, A., A&A, 260, L7

Murdin, P., Jauncey, D. L., Haynes, R. F., Lerche I., Nicolson, G. D., Holt, S. S., Kaluzienski, L. J., 1980, A&A, 87, 292

Oosterbroek, T., van der Klis, M., Kuulkers, E., van Paradijs J., Lewin, W. G. H., 1995, A&A, 297, 141

Predehl P. & Schmitt J. H. M. M., 1995, A&A, 293, 889

Shirey R. E., Bradt, H. V., Levine, A. M., Morgan, E. H., 1996, ApJL, 469, L21

Shirey R. E., 1998, Ph.D. Thesis, MIT

Shirey R. E., Bradt, H. V., Levine, A. M., 1999a, ApJ, 517, 472

Shirey R. E., Levine, A. M., Bradt, H. V., 1999b, ApJ, 524, 1048

Stella, L., & Vietri, M. 1999, Phys. Rev., 82, L17

Stewart, R. T., Nelson, G. J., Penninx, W., Kitamoto, S., Miyamoto, S., Nicolson, G. D., 1991, MNRAS, 1991, 253

Stewart, R. T., Caswell, J. L., Haynes, R. F., Nelson, G. J., 1993, MNRAS, 261, 593

Strohmayer, T. E., Zhang, W., Swank, J. H., Smale, I., Titarchuk, L., Day, C., Lee, U. 1996, ApJ, 469, L9

Tennant, A. F., Fabian, A. C., Shafer, R. A., 1986a, MNRAS, 219, 871

Tennant, A. F., Fabian, A. C., Shafer, R. A., 1986b, MNRAS, 221, 27P

Tennant, A. F., 1987, MNRAS, 226, 971

Titarchuk L., 1994, ApJ, 434, 570

Titarchuk, L., Lapidus, I., Muslimov, A. 1998, ApJ, 499, 315

Toor, A., 1977, ApJL, 174, L57

Turner, T. J., Done, C., Mushotzky, R., Madejski G., 1992, ApJ, 391, 102

Whelan, J. A. J., et al., 1977, MNRAS, 181, 259

**TABLE**

Table 1: In the first column we report the label number associated to the intervals in which we divided our observation, in the second column the start and end times (in second) for each interval referred to August 1 15:59:54.5 UT, the start time of MECS. The average hardness ratio is the count rate in the energy band 3–7 keV divided by the count rate in 1–3 keV. The fluxes are in units of  $10^{-8}$  ergs  $\text{cm}^{-2}$   $\text{s}^{-1}$ . The luminosity is in units of  $10^{38}$  ergs  $\text{s}^{-1}$ , assuming a distance of the source of 5.5 kpc (Case & Bhattacharya, 1998). The 7th column indicates the intervals where the LECS data are available.

Interval	Start–End time (s)	Average hard color	Flux 2.5–25 keV	Flux 0.1–100 keV	Luminosity 0.1–100 keV	LECS data
1	0–3300	$0.61 \pm 0.04$	1.51	2.49	0.94	No
2	3700–4819	$0.62^{+0.04}_{-0.01}$	2.00	3.25	1.23	No
3	4820–5814	$0.73 \pm 0.03$	2.88	4.35	1.65	No
4	5815–6300	$0.80 \pm 0.02$	3.27	4.80	1.82	No
5	7500–9500	$0.61^{+0.04}_{-0.01}$	2.00	3.26	1.24	No
6	9511–34322	$0.53 \pm 0.04$	1.24	2.24	0.85	Yes
7	34326–58831	$0.57 \pm 0.04$	1.35	2.34	0.89	Yes
8	58832–69829	$0.60 \pm 0.02$	1.62	2.69	1.02	No

Table 2: Results of the fit of Cir X–1 spectra during the flare in the energy band 0.1–100 keV, with a comptonized spectrum modeled by Comptt, a power law and an absorption edge. Uncertainties are at 90% confidence level for a single parameter.  $kT_0$  is the temperature of the seed photons for the Comptonization,  $kT_e$  is the electron temperature,  $\tau$  is the optical depth of the scattering cloud using a spherical geometry,  $R_W$  is the Wien radius of the seed photons in km and  $f_{bol}$  is the intrinsic flux of the comptonized model in unit of ergs  $\text{cm}^{-2} \text{ s}^{-1}$ . The power law normalization is in units of photons  $\text{keV}^{-1} \text{ cm}^{-2} \text{ s}^{-1}$  at 1 keV. F–Test indicates the probability of chance improvement when the power law is included in the spectral model.

Interval	1	2	3	4	5
$N_H$ ( $\times 10^{22} \text{ cm}^{-2}$ )	1.740 (frozen)				
$E_{edge}$ (keV)	$8.387 \pm 0.069$	$8.25 \pm 0.14$	$8.38 \pm 0.29$	$8.57 \pm 0.18$	$7.83^{+0.19}_{-0.15}$
$\tau_{edge}$	$0.609 \pm 0.079$	$0.73^{+0.21}_{-0.18}$	$0.31 \pm 0.12$	$0.50 \pm 0.16$	$0.56^{+0.19}_{-0.15}$
$kT_0$ (keV)	$0.397 \pm 0.024$	$0.422 \pm 0.019$	$0.431 \pm 0.021$	$0.448^{+0.034}_{-0.028}$	$0.400 \pm 0.030$
$kT_e$ (keV)	$0.921^{+0.056}_{-0.050}$	$1.026^{+0.096}_{-0.063}$	$1.043^{+0.051}_{-0.044}$	$1.089^{+0.077}_{-0.072}$	$0.901^{+0.078}_{-0.046}$
$\tau$	$16.6^{+1.9}_{-1.6}$	$14.2^{+1.6}_{-1.8}$	$15.9 \pm 1.3$	$15.6^{+2.0}_{-1.7}$	$17.4^{+2.0}_{-2.4}$
$N_{\text{comp}}$	$34.1^{+3.2}_{-4.1}$	$38.3^{+4.0}_{-4.6}$	$43.3^{+3.2}_{-3.3}$	$42.1^{+4.8}_{-4.3}$	$45.3^{+4.8}_{-5.6}$
$f_{bol} (\times 10^{-8})$	5.5	6.2	8.9	9.4	7.2
$R_W$ (km)	$140 \pm 20$	$142 \pm 17$	$151 \pm 17$	$144 \pm 25$	$156 \pm 28$
Photon index	$3.27^{+0.76}_{-0.83}$	3.30 (frozen)	3.30 (frozen)	3.30 (frozen)	3.30 (frozen)
Power–Law N	$1.7^{+12.1}_{-1.6}$	$< 1.14$	$< 0.78$	$< 1.3$	$1.61^{+0.85}_{-0.93}$
$\chi^2/\text{d.o.f.}$	231/234	238/259	224/200	228/252	190/232
F–Test	$\sim 0$	0.3	1	1	$2 \times 10^{-3}$

Table 3: Results of the fit of Cir X-1 spectra out the flare in the energy band 0.1–100 keV, with a comptonized spectrum modeled by Comptt, a power law, a gaussian emission line and an absorption edge. Uncertainties are at 90% confidence level for a single parameter. Definitions are as in Table 2.  $EQW_{Fe}$  indicates the equivalent width of the gaussian emission line,  $E_{Fe}$  the centroid of the emission iron line and  $I_{Fe}$  is the normalization of the emission iron line in units of photons  $\text{cm}^{-2} \text{ s}^{-1}$ .

Interval	6	7	8
$N_H (\times 10^{22} \text{ cm}^{-2})$	$1.727^{+0.113}_{-0.048}$	$1.737^{+0.181}_{-0.075}$	1.740 (frozen)
$E_{edge}$ (keV)	$8.495 \pm 0.053$	$8.477^{+0.076}_{-0.066}$	$8.594^{+0.082}_{-0.073}$
$\tau_{edge}$	$1.02 \pm 0.13$	$0.844^{+0.053}_{-0.167}$	$0.73 \pm 0.11$
$kT_0$ (keV)	$0.378^{+0.010}_{-0.013}$	$0.382^{+0.016}_{-0.024}$	$0.420^{+0.022}_{-0.015}$
$kT_e$ (keV)	$0.839^{+0.025}_{-0.029}$	$0.859^{+0.025}_{-0.056}$	$0.911^{+0.039}_{-0.046}$
$\tau$	$16.67^{+0.92}_{-0.76}$	$17.2^{+2.0}_{-1.3}$	$16.0^{+1.4}_{-1.1}$
$N_{\text{comp}}$	$40.9^{+3.0}_{-2.3}$	$38.2^{+5.2}_{-3.3}$	$36.3^{+2.4}_{-3.4}$
$f_{bol} (\times 10^{-8})$	5.5	5.4	5.8
$R_W$ (km)	$161 \pm 13$	$152 \pm 22$	$134 \pm 16$
Photon index	$3.16^{+0.48}_{-0.39}$	$3.34^{+0.50}_{-0.43}$	$3.37^{+0.50}_{-0.47}$
Power-Law N	$1.5^{+4.2}_{-1.0}$	$2.5^{+7.2}_{-1.8}$	$2.8^{+8.5}_{-2.1}$
$E_{Fe}$ (keV)	$6.70 \pm 0.10$	$6.82^{+0.14}_{-0.28}$	$6.31^{+0.30}_{-0.61}$
$\sigma_{Fe}$ (keV)	$< 0.24$	$< 0.47$	$0.50^{+0.51}_{-0.30}$
$I_{Fe}$	$(1.34^{+0.60}_{-0.56}) \times 10^{-3}$	$(2.8^{+7.0}_{-1.6}) \times 10^{-3}$	$(5.7^{+13.6}_{-3.4}) \times 10^{-3}$
$EQW_{Fe}$ (eV)	46.1	100.	82.2
$\chi^2/\text{d.o.f.}$	685/591	651/609	141/194
F-Test	$\sim 0$	$\sim 0$	$\sim 0$

## FIGURE CAPTIONS

**Figure 1:** Upper panel: Cir X-1 light curve in the energy band 1.8–10 keV (MECS data); the selected time intervals are indicated at the top of the panel. Lower panel: The ratio of the count rate in the energy band 3–7 keV with respect to that in 1–3 keV. The bin time is 137 s.

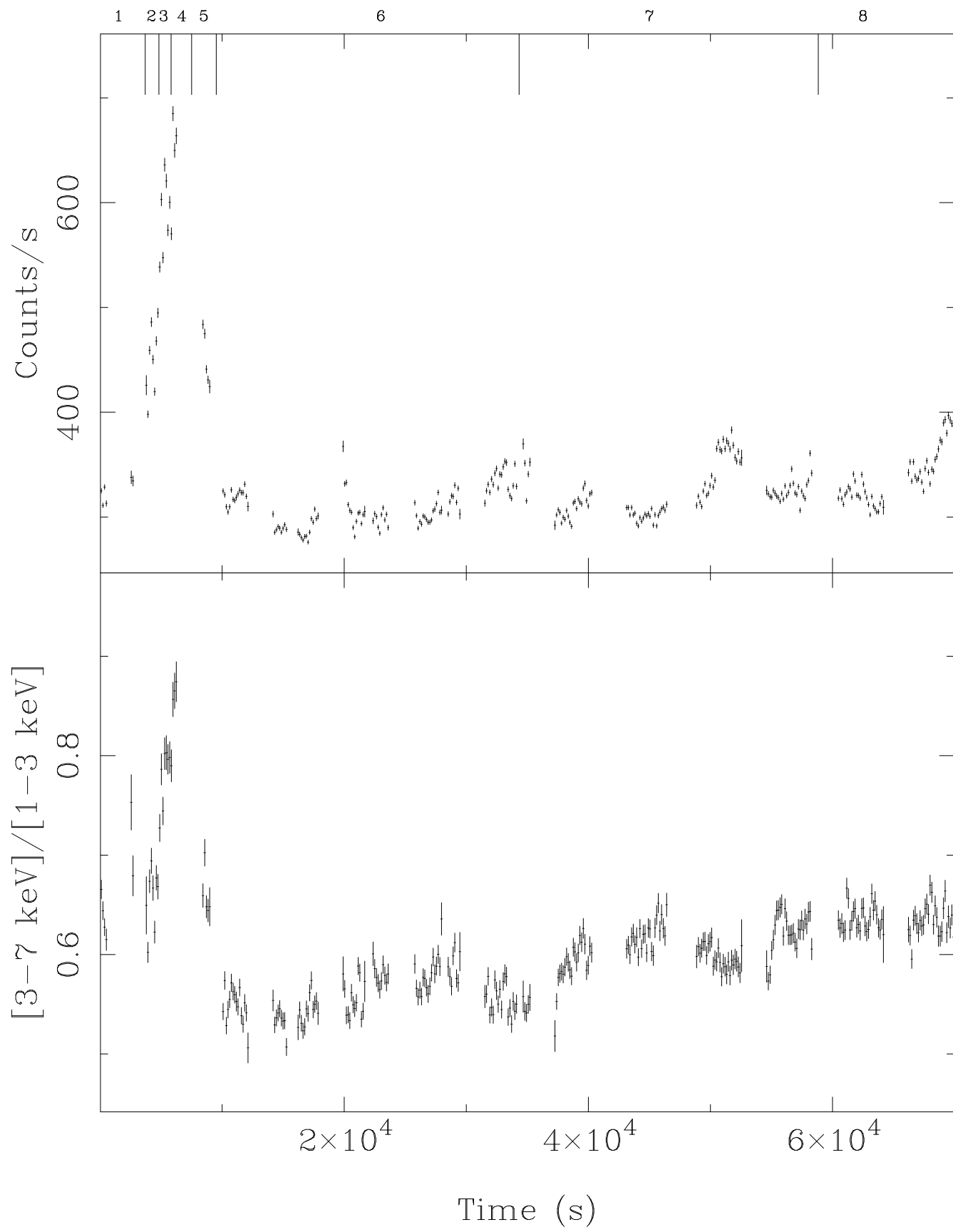
**Figure 2:** The color-color diagram of Cir X-1. The hard color is the ratio of the count rate in the energy band 7–10 keV with respect to that in the band 3–7 keV, while the soft color is the ratio (3–7 keV)/(1–3 keV). The bin time is 137 s. The main variation visible in the diagram is due to the observed flare.

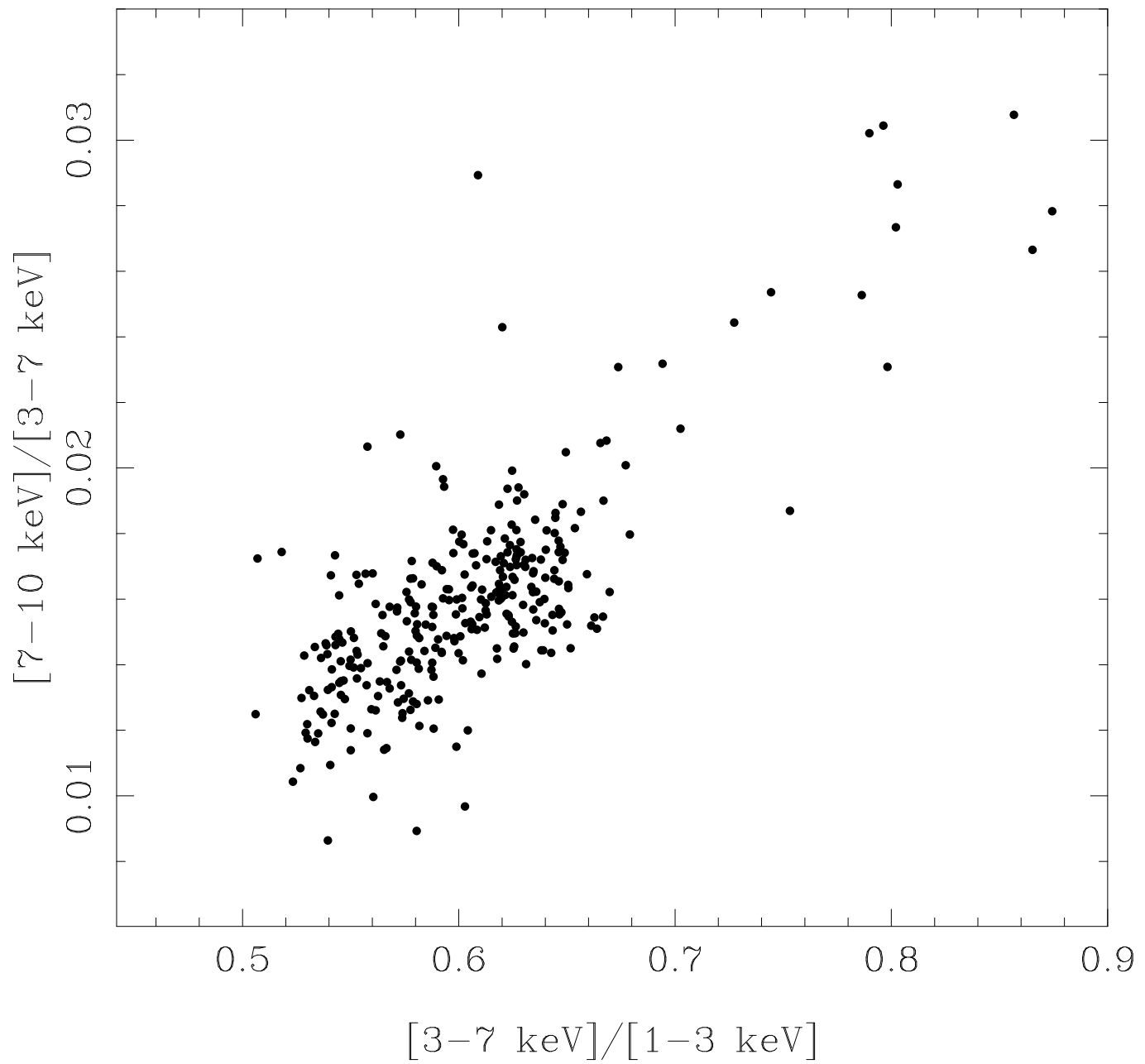
**Figure 3:** Energy spectra (0.1–100 keV) of Cir X-1 for intervals 6 (out of the flare, left side) and 4 (peak of the flare, right side). Data and the corresponding best fit model (see Tab. 2 and 3) are shown in the upper panels, residuals in units of  $\sigma$  with respect to the best fit model are shown in the lower panels.

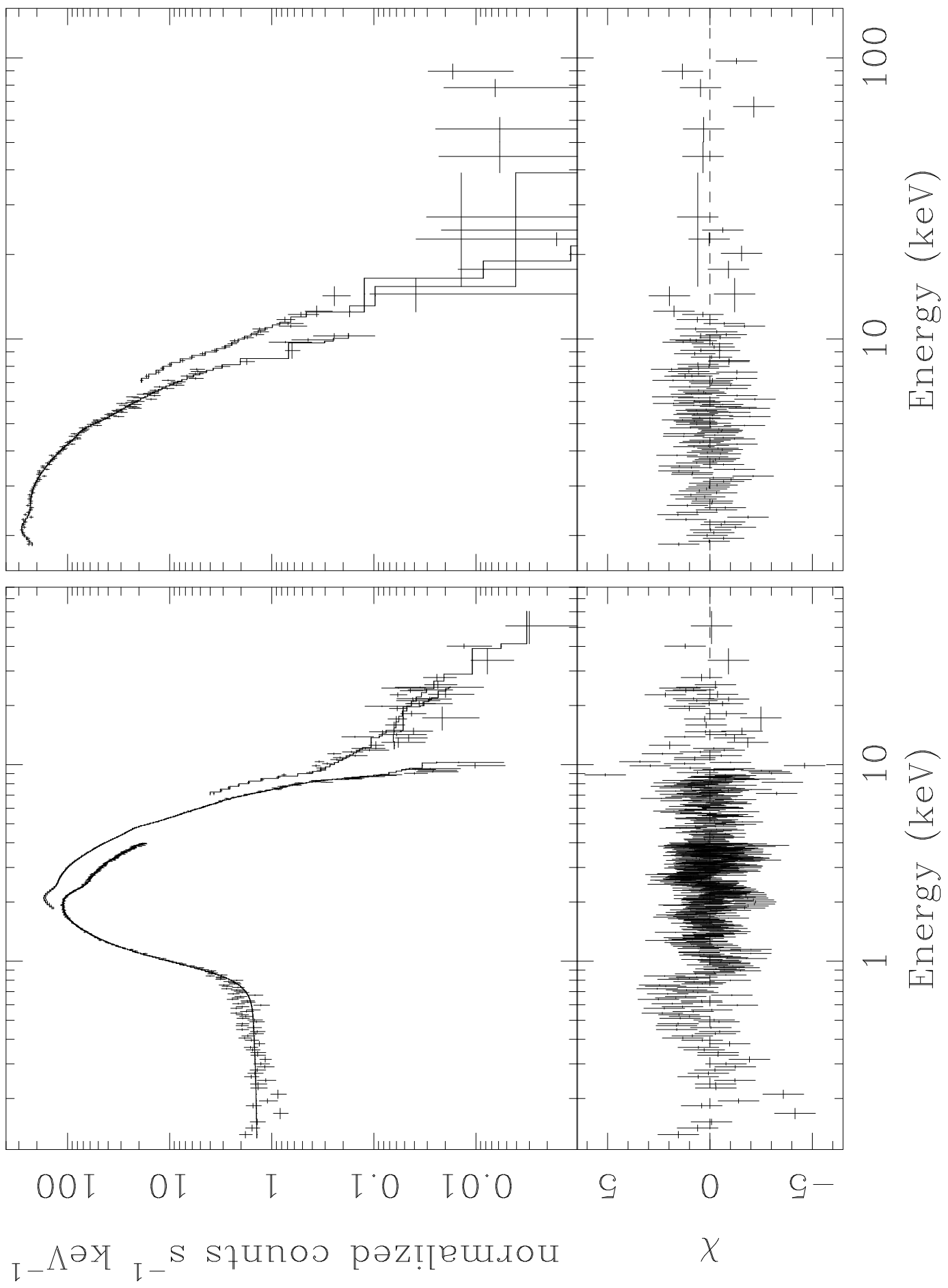
**Figure 4:** Left Panel: Unfolded spectrum and the best fit model, shown in this figure as a solid line, for interval 6. The single components of the model are also shown, namely the *Comptt* (dashed line), Power Law (dotted line) and iron emission line (dot-dashed line). The absorption edge at 8.4 keV is visible. Right Panel: Unfolded spectrum and the best fit model, shown as a solid line, for interval 4. The absorption edge at 8.4 keV is visible.

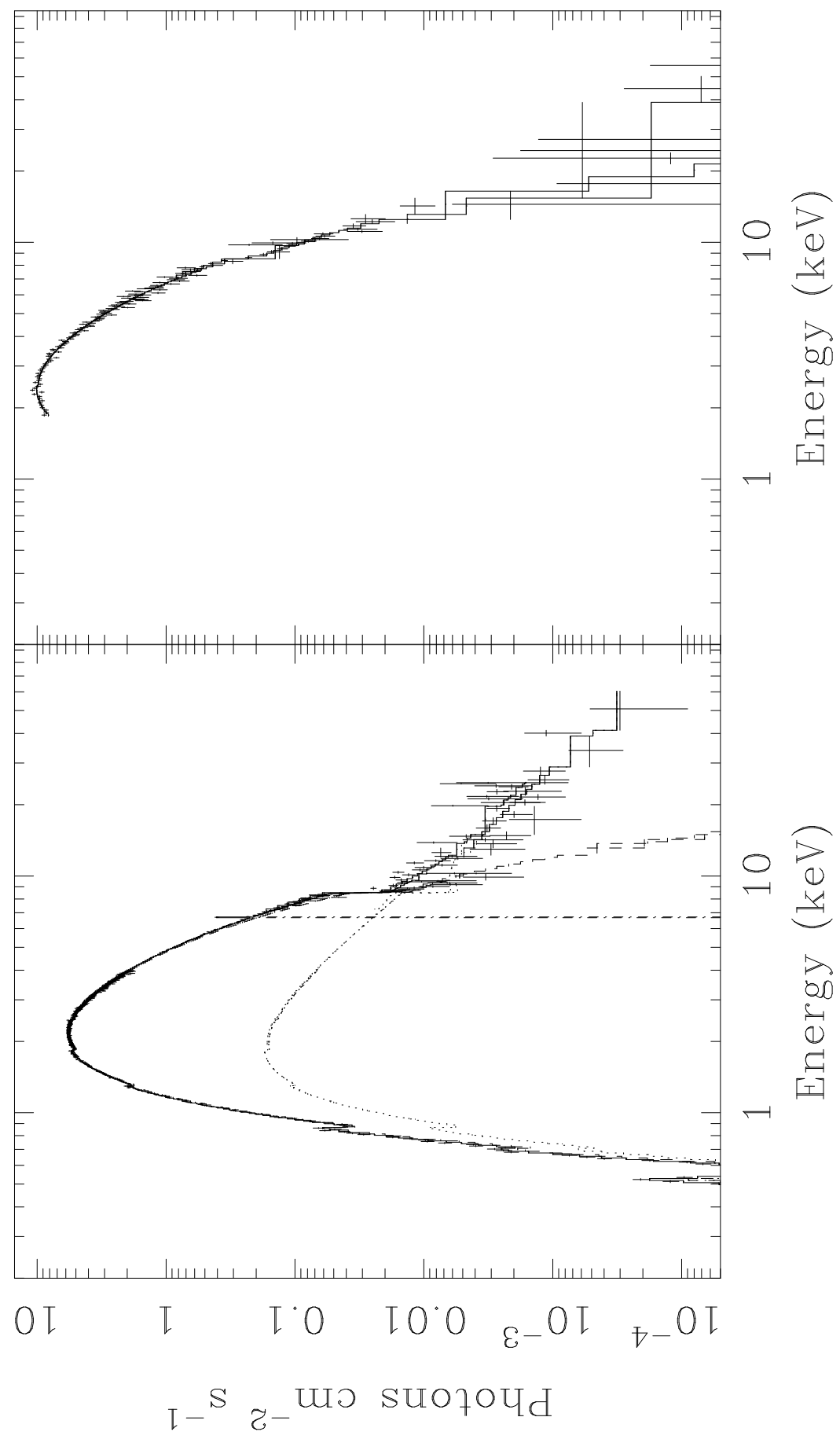
**Figure 5:** Seed-photon temperature (upper panel) and electron temperature (lower panel) of the comptonized spectrum as a function of the time, where the time values are the centers of each interval (see Tab. 1).

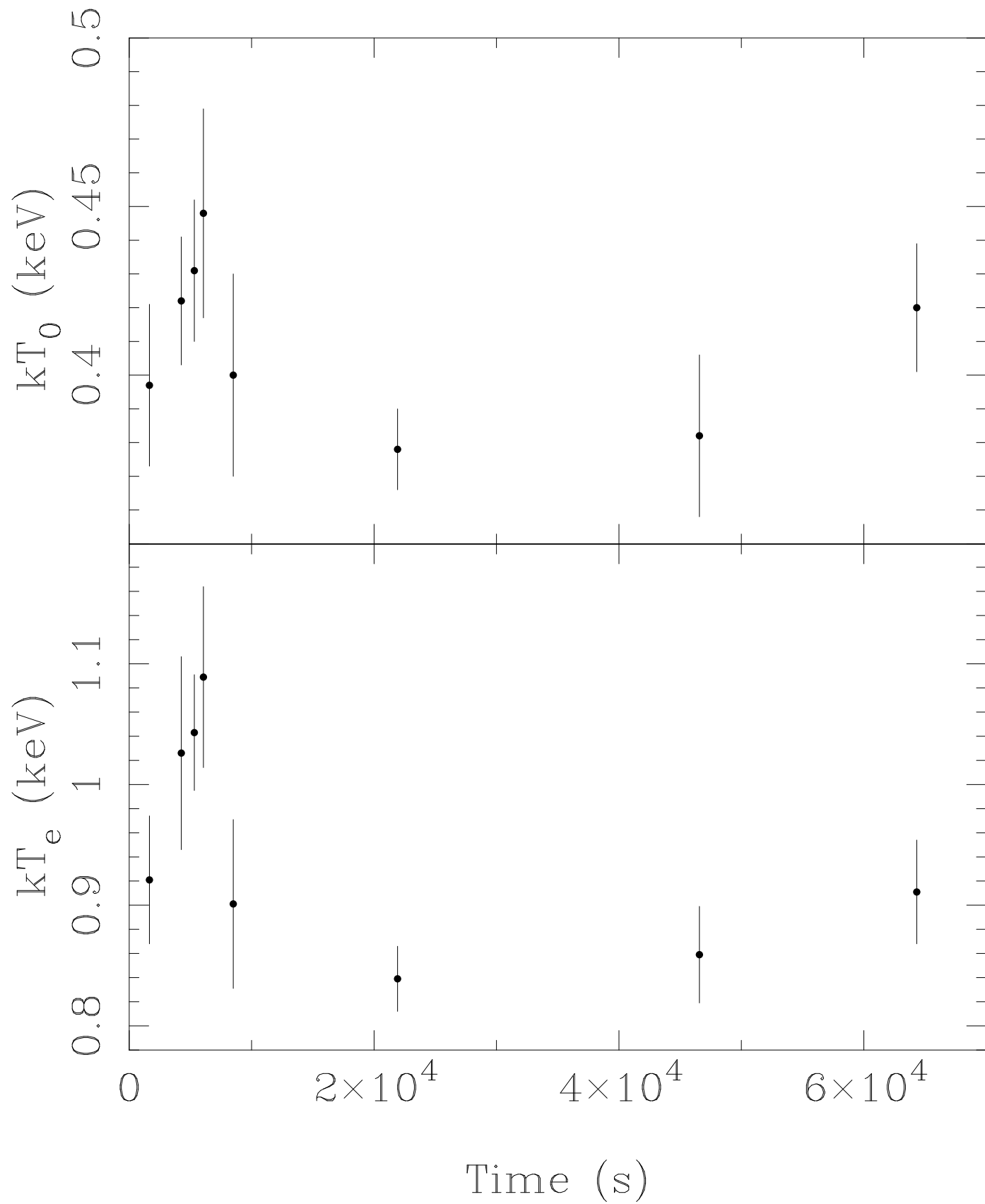
**Figure 6:** The electron temperature of the comptonizing region as a function of the seed-photon temperature. The solid line is a linear fit, with a slope of  $\sim 3.2$ .

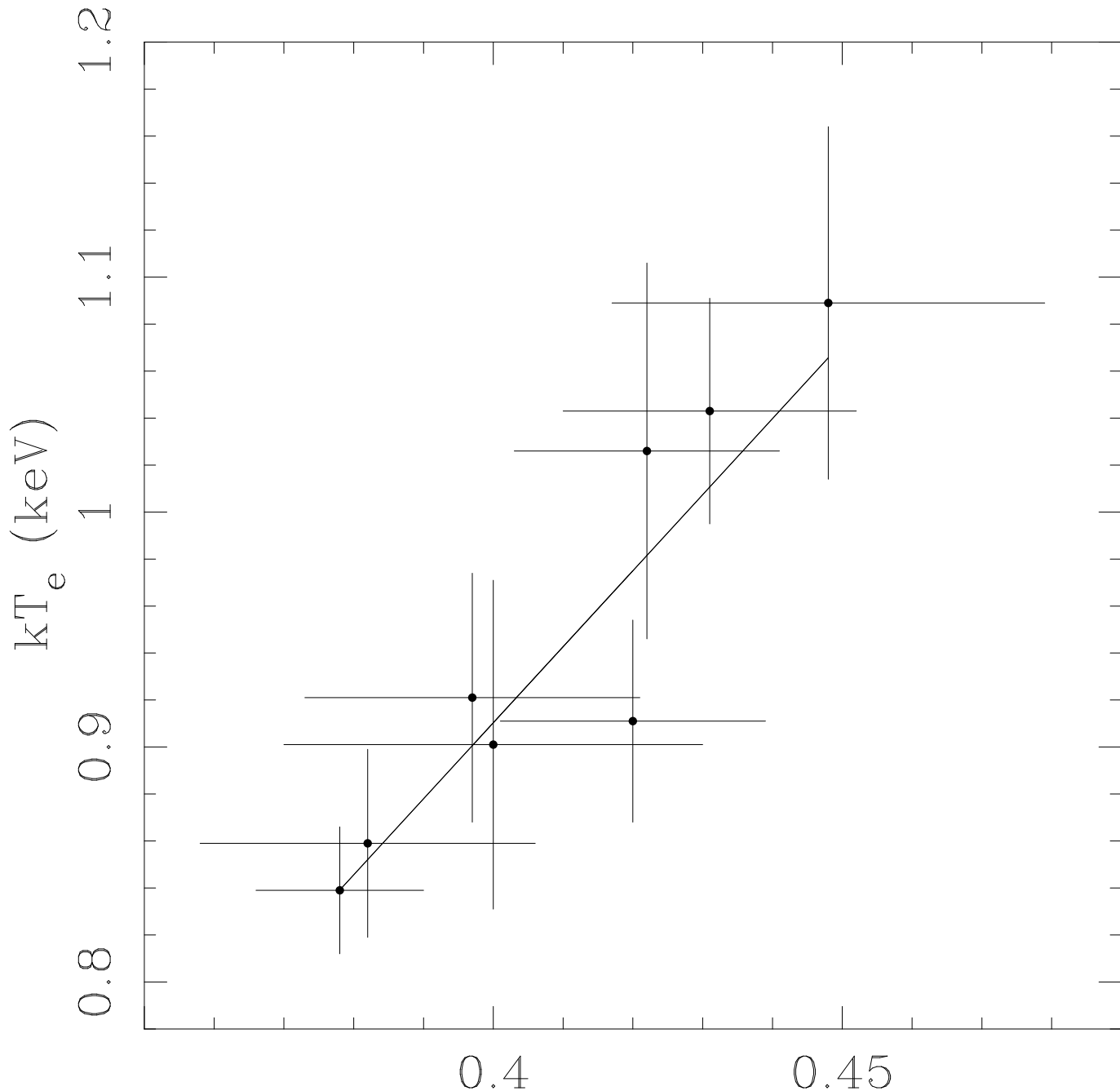












$$kT_0 \text{ (keV)}$$